IOPscience iopscience.iop.org

Home Search Collections Journals About Contact us My IOPscience

Intrinsic magnetic properties of the iron-rich $ThMn_{12}$-structure alloys $R(Fe_{11}Ti)$; R=Y, Nd, Sm, Gd, Tb, Dy, Ho, Er, Tm and Lu

This article has been downloaded from IOPscience. Please scroll down to see the full text article.

1989 J. Phys.: Condens. Matter 1 755

(http://iopscience.iop.org/0953-8984/1/4/009)

View the table of contents for this issue, or go to the journal homepage for more

Download details:
IP Address: 171.66.16.90
The article was downloaded on 10/05/2010 at 17:03

Please note that terms and conditions apply.

J. Phys.: Condens. Matter **1** (1989) 755–770. Printed in the UK

Intrinsic magnetic properties of the iron-rich $ThMn_{12}$-structure alloys $R(Fe_{11}Ti)$; R = Y, Nd, Sm, Gd, Tb, Dy, Ho, Er, Tm and Lu

Bo-Ping Hu, Hong-Shuo Li, J P Gavigan and J M D Coey
Department of Pure and Applied Physics, Trinity College, Dublin 2, Ireland

Received 27 May 1988, in final form 14 September 1988

Abstract. Magnetic properties of the series of $ThMn_{12}$-structure intermetallic compounds $R(Fe_{11}Ti)$ have been determined for rare earths from Nd to Lu plus Y. The highest Curie temperature (607 K) is for R = Gd, and R–Fe exchange interactions are much stronger for light rare earths than for heavy ones. The temperature dependence of the iron sublattice magnetisation and anisotropy are determined for the Y and Lu compounds. Spin reorientation transitions are found as a function of temperature for the rare earths with a negative second-order Stevens coefficient α_J(Nd, Tb, Dy), and a set of crystal-field parameters is derived to account for the transitions in a consistent way. A sharp increase in magnetisation observed for $Sm(Fe_{11}Ti)$ below 130 K in a field of about 10 T applied perpendicular to the easy direction indicates that J-mixing may be important for Sm^{3+}. Compared with $R_2Fe_{14}B$, the iron anisotropy in $R(Fe_{11}Ti)$ is greater, and the rare-earth anisotropy is much weaker at low temperature, with the opposite sign for the rare-earth crystal-field coefficient A_{20}. The average iron moment is 1.7 μ_B in $R(Fe_{11}Ti)$ at 4.2 K; Mössbauer spectra are analysed to yield the average moments on each site. Limits set by the intrinsic magnetic properties on the performance of magnets made from these families of alloys are discussed.

1. Introduction

The discovery of the iron-rich ternary phase $Nd_2Fe_{14}B$ in 1983 [1–3] gave new impetus to the search for iron-rich rare-earth intermetallic compounds for possible application as permanent magnets. Interest has recently focused on pseudo-binaries with the $ThMn_{12}$ structure, $R(Fe_{12-x}M_x)$. Although the pure end-member RFe_{12} does not exist for any rare earth, the structure has been stabilised for $x \geqslant 1$ and M = Ti, V, Cr, Mo, W and Al [4–7]. The samarium compound $SmFe_{10}Ti$ is reported to have strong uniaxial anisotropy and a Curie temperature (600 K) [8–9] comparable to that of $Nd_2Fe_{14}B$ (589 K) [10].

The $ThMn_{12}$ structure, illustrated in figure 1, is tetragonal with space group I4/mmm and $Z = 2$. The rare earth occupies the single 2*a* thorium site (point symmetry 4/mmm) while the transition elements are distributed over the three manganese sites, 8*f*, 8*i*, 8*j*. Iron is found to occupy 8*f* and 8*j* sites fully in $Y(Fe_{11}Ti)$, while the 8*i* site is populated by a mixture of Fe and Ti [11].

In order to develop an understanding of the intrinsic magnetic properties of rare-earth iron compounds with this structure, we have examined a wide range of alloys with $x = 1$ and M = Ti. Our approach is to use the compounds with non-magnetic rare earths

0953-8984/89/040755 + 16 $02.50 © 1989 IOP Publishing Ltd

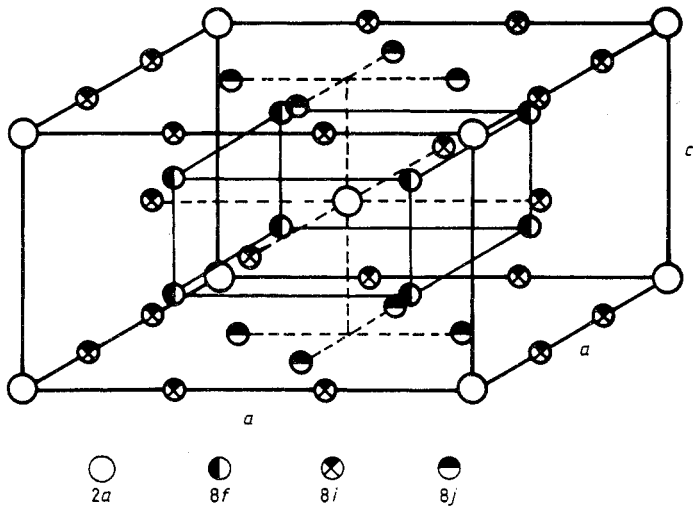

Figure 1. The crystal structure of $ThMn_{12}$.

(Y, Lu) to establish the magnetisation, exchange and anisotropy of the iron sublattice, then deduce R–Fe exchange from the Curie points of the rest of series, and finally establish a crystal-field model for the anisotropy of the 4f sublattice from measurements of spin reorientations as a function of temperature or applied field together with point charge calculations to estimate the ratios of crystal-field terms of the same order. The crystal-field Hamiltonian at the *2a* site takes the comparatively simple form [12]

$$H_{CF} = B_{20}\hat{o}_{20} + B_{40}\hat{o}_{40} + B_{44}\hat{o}_{44} + B_{60}\hat{o}_{60} + B_{64}\hat{o}_{64} \tag{1}$$

where B_{nm} are crystal-field parameters depending on the rare earth and $\hat{o}_{nm}$ are the Stevens operators.

The anisotropy of the rare-earth sublattice may be described by the phenomenological expression

$$E_R^a = K_1 \sin^2\theta + (K_2 + K_2' \cos 4\varphi)\sin^4\theta + (K_3 + K_3' \cos 4\varphi)\sin^6\theta \tag{2}$$

where θ and φ are the polar angles for the sublattice magnetisation relative to the crystallographic axes. The relations between the K_i for the rare earth and the B_{nm} are [13]

$$K_1 = -[(3/2)B_{20}\langle\hat{o}_{20}\rangle + 5B_{40}\langle\hat{o}_{40}\rangle + (21/2)B_{60}\langle\hat{o}_{60}\rangle] \tag{3a}$$

$$K_2 = (7/8)[5B_{40}\langle\hat{o}_{40}\rangle + 27B_{60}\langle\hat{o}_{60}\rangle] \tag{3b}$$

$$K_2' = (1/8)[B_{44}\langle\hat{o}_{40}\rangle + 5B_{64}\langle\hat{o}_{60}\rangle] \tag{3c}$$

$$K_3 = -(231/16)B_{60}\langle\hat{o}_{60}\rangle \tag{3d}$$

$$K_3' = -(11/16)B_{64}\langle\hat{o}_{60}\rangle \tag{3e}$$

which are valid in the $R(Fe_{11}Ti)$ system where the crystal field is considered as a perturbation on the rare-earth iron exchange interactions. The magnetic structure at any given temperature or applied field B^{app} is deduced by solving the coupled equations

describing the iron and rare-earth sublattices [14]

$$E_{Fe} = E^{a}_{Fe} - (\boldsymbol{B}^{ex}_{Fe} + \boldsymbol{B}^{app}) \cdot N_{Fe}\langle \boldsymbol{m} \rangle \tag{4a}$$

$$H_R = H_{CF} - \{[2(g_J - 1)/g_J]\boldsymbol{B}^{ex}_{R} - \boldsymbol{B}^{app}\} \cdot N_R g_J \boldsymbol{J} \mu_B \tag{4b}$$

which are linked by the intersublattice molecular field B^{ex}. Here $\langle \boldsymbol{m} \rangle$ and $-g_J\langle \boldsymbol{J} \rangle \mu_B$ are the average atomic moments of the iron and rare earth, N_{Fe} and N_R are the numbers of atoms per unit volume, and E^{a}_{Fe} is the iron anisotropy energy represented by a term $K_1(\mathrm{Fe}) \sin^2 \theta$. The factor $2(g_J - 1)/g_J$ is included because the exchange field acts on the spin magnetic moment of the 4f shell. It should be modified if there is any significant J-mixing (e.g. for Sm^{3+}). The exchange fields are given in terms of the molecular field coefficient n_{RFe}

$$\boldsymbol{B}^{ex}_{R} = n_{RFe} N_{Fe} \langle \boldsymbol{m} \rangle \tag{5a}$$

and

$$\boldsymbol{B}^{ex}_{Fe} = -n_{RFe}[2(g_J - 1)/g_J] N_R g_J \langle \boldsymbol{J} \rangle \mu_B . \tag{5b}$$

Previous magnetic measurements on $R(Fe_{10}V_2)$ compounds with R = Y, Gd or Lu [5] and $Y(Fe_{11}Ti)$ [11] indicate that the anisotropy of the iron sublattice favours the crystallographic c axis (K_1 is positive). Magnetisation measurements for other rare earths as well as ^{155}Gd Mössbauer results [6] suggest that the second-order term B_{20} in the rare-earth crystal field for ions having a positive second-order Stevens coefficient α_J (Sm, Er, Tm, Yb) will also favour the c axis whereas for ions having a negative α_J the c axis should be hard direction from rare-earth's point of view. The signs of B_{20} are therefore opposite to those of corresponding members of $R_2Fe_{14}B$ series [15], where the c axis is easy for ions with α_J negative (Pr, Nd, Tb, Dy, Ho); K_1 for the iron sublattice is also positive.

Spin reorientation transitions are expected when the balance of competing iron and rare-earth anisotropies changes as a function of temperature. Transitions from the plane (perpendicular to the c axis) to the c axis are observed in $R_2Fe_{14}B$ on increasing the temperature for R = Er, Tm, and Yb at 325 K, 314 K, and 115 K, respectively. The corresponding transitions in $R(Fe_{11}Ti)$ with R = Nd, Tb, Dy, Ho turn out to be more complicated because of the importance of terms in the crystal field other than $B_{20}\hat{o}_{20}$ in (1). We have already reported that the spin reorientation in $Dy(Fe_{11}Ti)$ has its onset at about 80 K, but is complete (i.e. $\boldsymbol{M} \parallel c$ axis) only above 210 K [16]. Here we extend and develop that analysis for the whole rare-earth series and include a discussion of a first-order transition found for $Sm(Fe_{11}Ti)$ as a function of applied field, which is similar to that reported for $Pr_2Fe_{14}B$ [17, 18]. The crystal-field analysis permits us to identify where optimum intrinsic magnetic properties may be found in the $R(Fe_{12-x}M_x)$ series.

2. Experimental methods

All the $R(Fe_{11}Ti)$ samples except R = Sm were prepared by arc melting 99.9% pure elements, and annealing the ingots in vacuum at about 850 °C for 2–4 d. X-ray diffraction only showed reflections from the $ThMn_{12}$-structure, except for the thulium compound which contained a little unreacted iron, and the neodymium compound which contained some Nd_2Fe_{17}. Attempts to prepare the La, Ce and Pr compounds were unsuccessful. The samarium compound was supplied by Rare Earth Products.

Curie temperatures were determined from magnetisation measured as a function of

Table 1. Crystallographic and magnetic data on $R(Fe_{11}Ti)$ compounds. The error for the data in each column is the same as that given for each first entry.

				M_s (μ_B/FU)		B_a (T)	
R in $R(Fe_{11}Ti)$	a (nm)	c (nm)	T_c (K)	4.2 K	290 K	4.2 K	290 K
Y	0.851 (2)	0.478 (3)	524 (3)	19.0 (2)	16.6 (2)	4.0 (3)	2.0 (3)
Nd	0.856	0.478	547		16.8	—	
Sm	0.854	0.478	584		17.1		10.5
Gd	0.850	0.477	607		12.5		
Tb	0.851	0.477	554	9.7	10.6	—	—
Dy	0.848	0.477	534	9.7	11.3	—	2.3
Ho	0.847	0.477	520				
Er	0.846	0.477	505	9.2	12.4	8.3	3.6
Tm	0.846	0.477	496				
Lu	0.846	0.477	488		15.7		2.2

temperature using a vibrating-sample magnetometer with a steady applied field $B_0 = 5$ mT. Curie temperatures are listed in table 1 together with the lattice parameters a and c. The measurements at low temperatures in a larger field $B_0 = 100$ mT on samples composed of fine powder dispersed randomly in epoxy resin were used to determine the spin reorientation transition temperatures.

Magnetisation curves on random and oriented polycrytalline samples were measured up to high field values at the High Field Magnet Laboratory of the University of Nijmegen, at the Service National des Champs Intenses and at the Laboratory Louis Néel, Grenoble. Oriented samples were made by mixing finely ground alloy powder with epoxy resin setting in a field of 1.5 T. Magnetisation curves measured with the applied field perpendicular to the orientation direction were used to determine the anisotropy field of the easy c axis compounds.

Mössbauer spectra were collected using a conventional constant acceleration spectrometer with a ^{57}Co source in rhodium matrix. Hyperfine fields are quoted relative to an α-Fe absorber at room temperature used to calibrate the spectrometer. Samples consisted of about 15 mg cm^{-2} of alloy powder mixed with icing sugar to obtain homogeneous and isotropic absorbers. For oriented absorbers, the powder was mixed with epoxy resin and set in a 1.5 T field. Spectra were fitted to six Lorentzian sextets by least-squares computer minimisation. Different linewidths were permitted for the outer, middle and inner pairs of lines [19]. An overall intensity constraint of 4 : 3 : 4 was applied to the 8*f*, 8*i* and 8*j* subspectra in view of the site preference determined in [11].

3. Results

The exchange interactions in the series can be deduced in the molecular-field approximation from the expression for the magnetic ordering temperature.

$$T_C = (1/2)[T_{Fe} + (T_{Fe}^2 + 4T_{RFe}^2)^{1/2}] \tag{6a}$$

where

$$T_{Fe} = n_{FeFe}N_{Fe}[4S^*(S^* + 1)\mu_B^2/3k] \tag{6b}$$

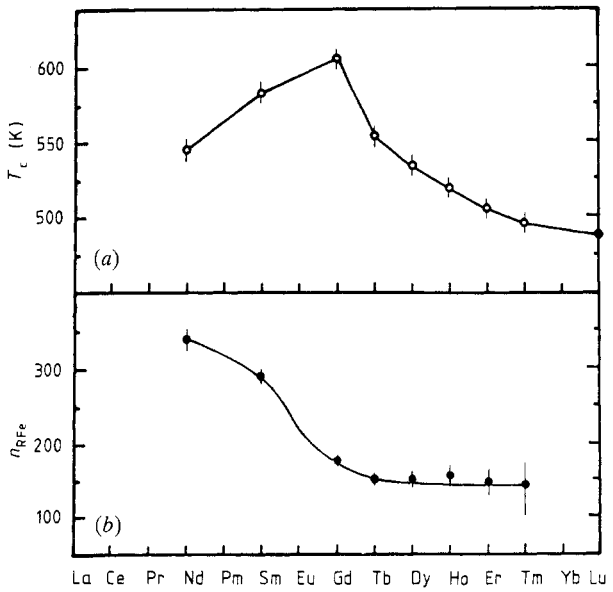

Figure 2. Curie temperature (*a*) and corresponding rare-earth–iron exchange coefficients (*b*) for the $R(Fe_{11}Ti)$ series.

and

$$T_{RFe} = n_{RFe}(N_{Fe}N_R)^{1/2}[2g_J[S^*(S^*+1)J_R(J_R+1)]^{1/2}\mu_B^2/3k] \qquad (6c)$$

Rare-earth–rare-earth exchange interactions are neglected, as they are expected to be less than 5% of the rare-earth–iron interactions. $2[S^*(S^*+1)]^{1/2}\mu_B$ is the effective moment of iron in the paramagnetic state, taken as $3.70\,\mu_B$ from a comparison of the paramagnetic susceptibility of related compounds (RFe_2, RFe_3, R_2Fe_{17}, $R_2Fe_{14}B$) [20, 21].

The iron–iron exchange coefficient is deduced from the Curie point of the lutetium compound (488 K) which has the same 5d/6s structure as the rest of the series and a non-magnetic $4f^{14}$ shell; $n_{FeFe} = 215\,\mu_0$. The Curie point of the yttrium compound is a little higher (524 K), as it is for both the R_2Fe_{17} and $R_2Fe_{14}B$ series [20, 15]. The extrapolated value of T_C for $La(Fe_{11}Ti)$ would be 495 K. The rare-earth–iron exchange coefficients deduced from T_C for the rest of the series are shown in figure 2. There is the familiar maximum in T_C for gadolinium, which has the largest spin moment, but n_{RFe} is roughly twice as large for the light rare earths as for the heavy rare earths. This behaviour of n_{RFe} is typical of isostructural series of compounds, and it has been discussed in terms of 4f–5d overlap [22].

Magnetisation curves for a few of the compounds at 290 K are shown in figure 3. All are effectively saturated in an applied field of 15 T. The corresponding magnetic moments per formula are included in table 1.

Figure 4 shows a variety of magnetic measurements on the yttrium compound. From the magnetisation curve of an oriented sample in the transverse direction (figure 4(*a*)) it is possible to deduce the anisotropy field B^a_{Fe} by plotting (B/M) versus M^2. This procedure takes account of imperfect orientation [23], and is more accurate than simply extrapolating the linear segment of the magnetisation curve to saturation. $K_1(Fe)$ is then deduced as $(1/2)B^a_{Fe}M_{Fe}$, where M_{Fe} is the iron sublattice magnetisation, the dependence of which is shown in figure 4(*c*). Finally, in figure 4(*d*) we show the temperature depen-

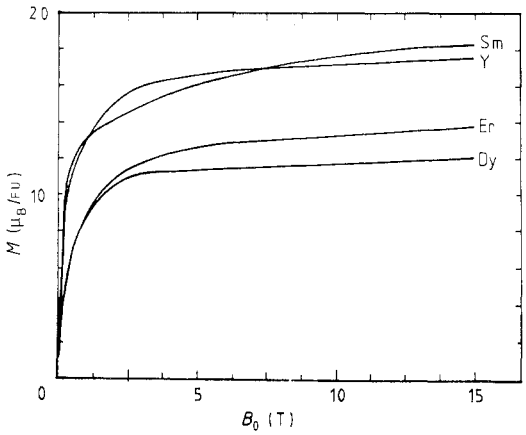

Figure 3. Magnetisation curves at 290 K for isotropic polycrystalline samples of $R(Fe_{11}Ti)$.

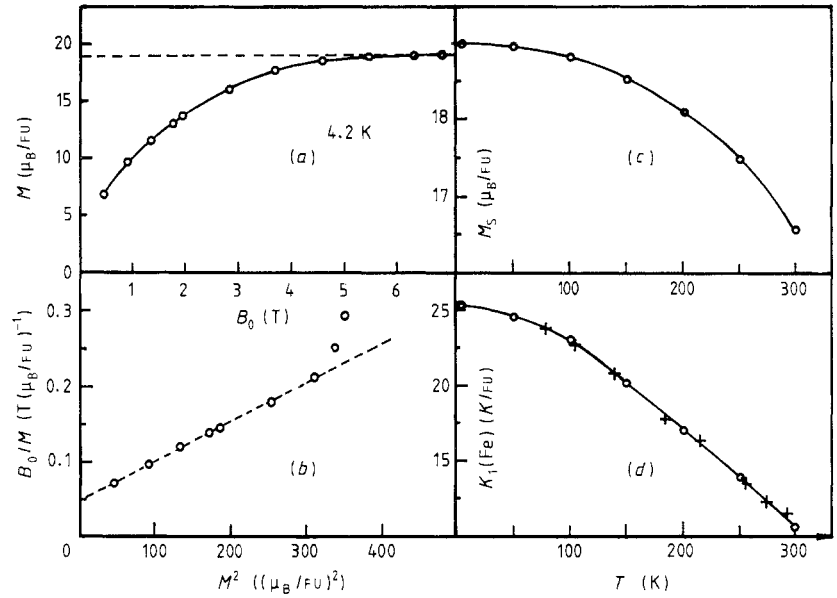

Figure 4. Some results for $Y(Fe_{11}Ti)$: (*a*) typical magnetisation curve on an oriented sample with the applied field perpendicular to the orientation direction; (*b*) the same data plotted to yield the anisotropy field; (*c*) spontaneous magnetisation as a function of temperature; and (*d*) the iron anisotropy constant $K_1(Fe)$ as a function of temperature. The crosses are independent data from [10], for the same compound.

dence of $K_1(Fe)$ deduced from the slopes of the curves like that in figure 4(*b*). The temperature dependence of B^a_{Fe} has also been measured more directly for $Y(Fe_{11}Ti)$ [11] using the singular point detection technique, and $K_1(Fe)$ deduced from their results is also shown in figure 4)(*d*) by the crosses, for comparison.

In figure 5 we shows the most interesting set of magnetisation curves for oriented samples as a function of temperature, those of the samurium compound. This is the only member of the series to show a sharp upturn in magnetisation as a function of applied field. This first-order magnetisation process (FOMP) below 130 K in an applied field of about 10 T is discussed in § 4.5.

Magnetisation variations as a function of temperature in an applied field of 100 mT are shown in figure 6. By comparison with the curves for Y, the data for Nd, Tb, Dy and

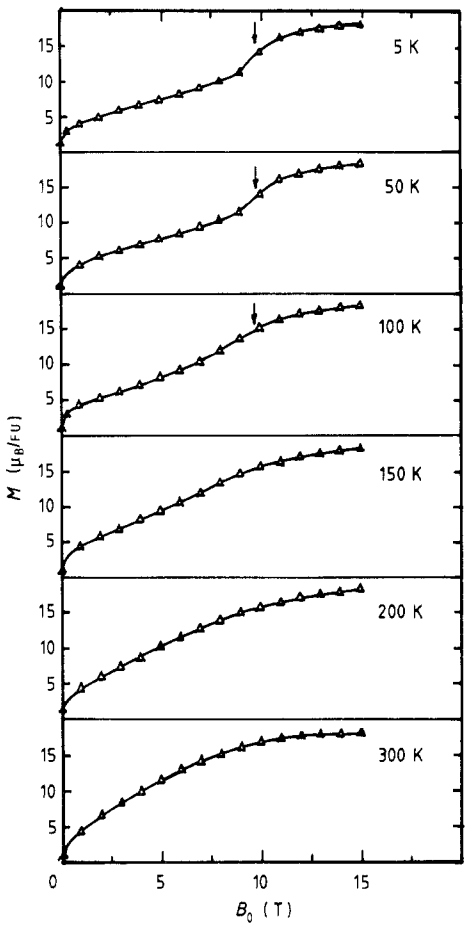

Figure 5. Magnetisation curve for an oriented $Sm(Fe_{11}Ti)$ sample in a transverse applied field.

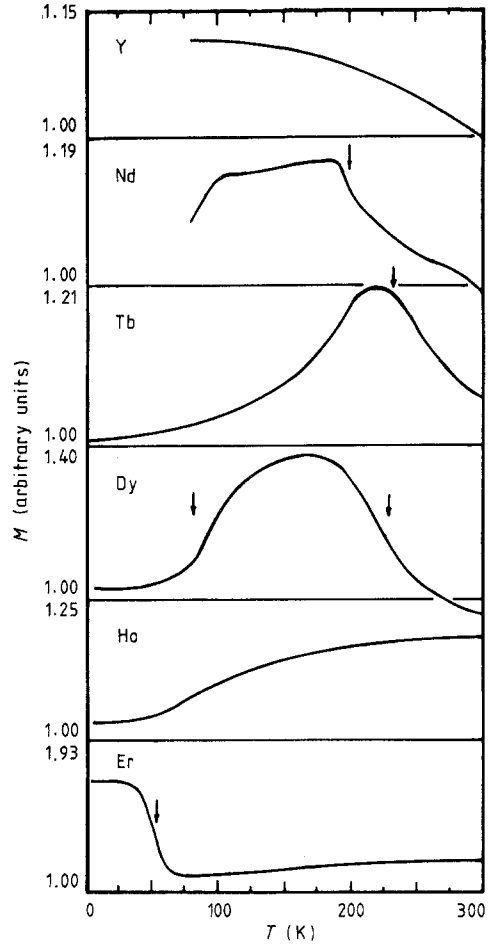

Figure 6. Magnetisation variation versus temperature measured in an applied field of 100 mT on randomly dispersed powder samples set in epoxy resin. The arrows mark the spin reorientation transitions.

Er all show an anomalous temperature variation which will be associated with spin reorientations. At room temperature and above, the uniaxial iron anisotropy usually determines the magnetisation direction but at lower temperature the rare-earth anisotropy may be dominant. Each compound is discussed separately in § 4.

Some typical ^{57}Fe Mössbauer spectra for the series at 80 K and at 290 K are shown in figure 7. The average hyperfine fields deduced from the fits are listed in table 2. The conversion factor from average hyperfine field $\langle B_{HF} \rangle$ to average iron moment $\langle m \rangle$ is 15.6 T/μ_B for $Y(Fe_{11}Ti)$ at both temperatures. Using this conversion throughout, the average iron moments are obtained. They range from 1.4–1.7 μ_B at 290 K, and the values extrapolated to zero range from 1.67μ_B for Lu to 1.86 μ_B for Dy.

A set of spectra as a function of temperature for an oriented $Dy(Fe_{11}Ti)$ absorber are shown in figure 8. The orientation at room temperature is imperfect because of the rather weak net uniaxial anisotropy. However, the spin reorientation below 240 K is

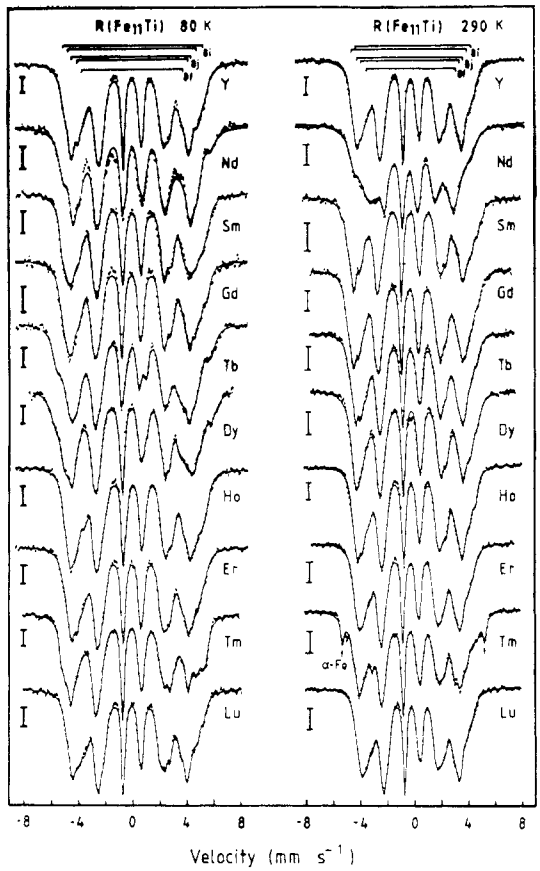

Figure 7. Mössbauer spectra for $R(Fe_{11}Ti)$ at 80 K and 290 K (vertical bars represent 1% of absorption).

evident from the increase in the relative intensities of the $\Delta m = 0$ transitions. It is also manifest as a step in the temperature variation of the average hyperfine field for each site, shown for Nd, Tb, and Dy in figure 9. The step is mainly due to a change in the 8*i* site hyperfine field, which is the largest of all the iron sites [7].

4. Analysis and discussion

4.1. 3d magnetism (R = Y, Lu)

The average iron moment in the $R(Fe_{11}Ti)$ series is rather small for a compound containing so much iron. At $T = 0$ K, average iron moments (in units of μ_B) are 1.73 and 1.67 for R = Y and Lu, respectively. Corresponding saturation inductions $\mu_0 M_S$ are 1.28 T and 1.24 T. We have no reason to suspect a non-collinear magnetic structure, because the magnetisation curves for the yttrium compound saturate normally (figure 3 and figure 4(*a*)) and the conversion factor from hyperfine field to moment (assuming collinear ferromagnetism) of 15.6 T/μ_B is close to that observed in other Y–Fe alloys [24]. In the fits to the ^{57}Fe Mössbauer spectra of the yttrium compound at 80 K, three

Table 2. Hyperfine fields for Fe sites and corresponding magnetic moments (conversion coefficient 15.6 T/μ_B) in R(Fe_{11}Ti) compounds at 80 K and 290 K. The error for the data in each column is the same as that given for each first entry.

		B_{HF} (T)				
R in R(Fe_{11}Ti)	T (K)	8*f*	8*i*	8*j*	$\langle B_{HF} \rangle$ (T)	μ_{Fe} (μ_B)
Y	80	23.4 (5)	30.8 (5)	27.3 (5)	26.8 (3)	1.72 (2)
	290	20.6	27.1	23.5	23.5	1.51
Nd	80	25.1	30.8	28.0	27.7	1.77
	290	18.6	26.4	20.7	21.5	1.38
Sm	80	24.8	32.5	28.7	28.3	1.81
	290	22.7	28.8	25.9	25.5	1.63
Gd	80	24.9	32.5	28.3	28.2	1.81
	290	22.2	29.1	25.4	25.3	1.62
Tb	80	24.9	33.9	28.4	28.6	1.83
	290	21.2	27.8	24.5	24.2	1.55
Dy	80	25.5	33.7	28.8	28.9	1.85
	290	22.2	27.4	24.4	24.4	1.56
Ho	80	23.8	31.3	27.6	27.3	1.75
	290	20.6	27.0	23.9	23.6	1.51
Er	80	23.2	30.8	27.1	26.7	1.71
	290	19.9	26.4	23.1	22.8	1.46
Tm	80	24.0	30.4	28.5	27.4	1.75
	290	21.0	26.5	23.2	23.3	1.50
Lu	80	22.3	29.6	26.1	25.7	1.65
	290	19.2	26.0	22.3	22.2	1.42

components are found with average hyperfine fields of 30.8, 27.3 and 23.4 T, with the 3:4:4 intensity constraint. On extrapolating to $T = 0$ K, these correspond to moments (in units of μ_B) of 1.99, 1.76 and 1.51. To assign these moments to the three sites, we consider nearest-neighbour environments. The numbers of nearest-neighbour sites for 8*f* are (2, 2, 4, 4), for 8*i* are (1, 4, 5, 4) and for 8*j* are (2, 4, 4, 2) where the numbers in brackets refer to 2*a*, 8*f*, 8*i* and 8*j* site neighbours, respectively. A quarter of 8*i* sites are occupied by titanium. So iron on 8*i* sites has 11.75 iron neighbours, while iron on both 8*f* and 8*j* sites has 9 iron nearest neighbours. The average Fe–Fe distances are 2.49, 2.69 and 2.57 Å for 8*f*, 8*i* and 8*j* sites, respectively. On the basis of iron coordination number and Fe–Fe distances, there is little doubt that the 8*i* site should have the largest moment. The Fe–Fe distances suggest that 8*f* iron should have the smallest moment and this is the assignment we have adopted in figure 9. The band calculations for YMn_{12} support this view [25]. However, Helmheldt and co-workers [26] have fitted a neutron powder diagram of Y($Fe_{10}V_2$) with the smallest moment on 8*j* sites, although they achieved a marginally better refinement of their data if all three iron moments are considered to be equal. Site occupancy and moment are correlated parameters in these refinements. Titanium in an alloy is more effective than yttrium or the other rare earths at reducing the iron moment; the critical concentration x_c for the appearance of magnetism in amorphous Fe_xM_{100-x} alloys is near 0.43 for M = Ti, but it is 0.36 for M = Y [27].

The uniaxial iron anistropy varies quite regularly as a function of temperature (figure 4(*d*)), unlike that of $R_2Fe_{14}B$ [28]. The value of K_1(Fe) at $T = 0$ is 2.0 MJ m^{-3}, compared with 0.8 MJ m^{-3} in $Y_2Fe_{14}B$. It seems likely that the anisotropy is mainly due to an orbital moment of iron on 8*i* sites, since the 8*i* hyperfine field is the one that shows a big

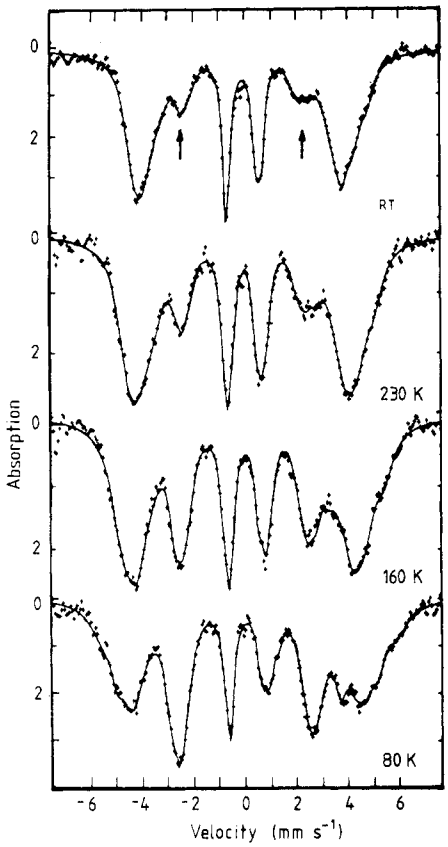

Figure 8. Mössbauer spectra for an oriented absorber ($Dy(Fe_{11}Ti)$) with the γ-ray parallel to the orientating field. The $\Delta m = 0$ transitions are marked by arrows.

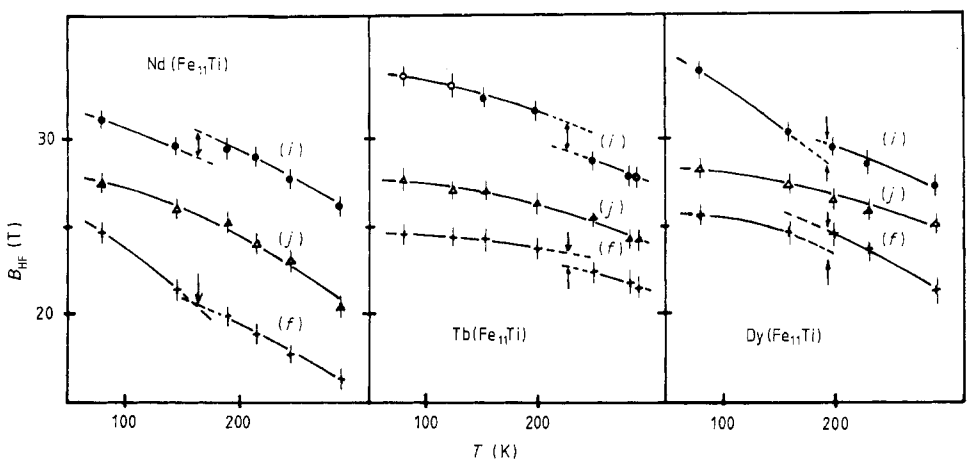

Figure 9. Hyperfine field at $8f$ (+), $8i$ (○) and $8j$ (△) sites in $R(Fe_{11}Ti)$ (R = Nd, Tb and Dy).

change at the spin reorientations (see § 4.4). Furthermore, the magnetovolume anomaly reported in [6] for $Er(Fe_{10}V_2)$ is smaller than that for $Er_2Fe_{14}B$ [29].

4.2. Magnetic structure

At room temperature, the spontaneous magnetisation of all the heavy rare-earth compounds is considerably less than that of the iron sublattice as measured for R = Y or Lu, whereas the spontaneous magnetisation for R = Nd or Sm is a little greater than that of the iron sublattice (table 1). This suggests the conventional coupling scheme of iron and rare-earth moments parallel for the light rare earths and antiparallel for the heavy rare earths. Only the value of the Nd moment differs from that expected in this scheme, which may be due to the presence of some low Curie temperature impurity with the Th_2Zn_{17} structure in this sample.

4.3. Rare-earth crystal field

X-ray diffraction and Mössbauer spectra on oriented samples showed a texture with easy *c*-axis anisotropy at room temperature for all the compounds except R = Nd and Tb. On the face of it, this is a surprising result since the second-order crystal field for any rare earth with negative α_J will favour an orientation of the rare-earth moment perpendicular to *c*-axis. However the electric field gradient at the 2*a* site in the $ThMn_{12}$ structure is quite small. Measurements of the field gradient at the ^{155}Gd nucleus can be scaled to yield A_{20}, and Buschow and co-workers [6] have found that the magnitude of A_{20} in $Gd(Fe_{10}M_2)$ compounds is about 20% of that in Gd compounds with the $Nd_2Fe_{14}B$ structure [6, 30]. The *iron* sublattice anisotropy is therefore the dominant term at room temperature for all rare earths except terbium.

In order to treat the anisotropy due to the rare-earth crystal-field Hamiltonian, (1), we need to reduce the number of free parameters. For different rare earths B_{20} can be related to the A_{20}-parameters by equations such as

$$B_{20} = \alpha_J \langle r^2 \rangle A_{20}. \tag{7}$$

No screening correction is made, so the A_{nm} should be practically constant throughout the series since they depend only on the crystal structure. Point charge calculations can be used to obtain values of A_{nm}, but these are notoriously unreliable insofar as absolute magnitudes are concerned [31]. An improvement is to take account of screening of individual rare-earth charge density in the Thomas–Fermi approximation [32, 33]. Such calculations give $A_{20} = -110\ \mathrm{K}\ a_0^{-2}$ for the series, where a_0 is the first Bohr radius. The point charge approach is moderately successful at predicting the ratio for terms of the same order [34]. With charges of $+3e$ and $-0.25e$ on R and Fe atoms respectively we find that $A_{44}/A_{40} = -2.4$ and $A_{64}/A_{60} = 1.6$. The ratios are the same for B_{44}/B_{40} and B_{64}/B_{60}. The problem of determining the magnetic structure as a function of temperature of applied field therefore reduces to the choice of A_{20}, A_{40} and A_{60}, since the other quantities in (1) are known.

4.4. Heavy rare earths

Taking the temperature variation of the iron sublattice magnetisation as that of $Y(Fe_{11}Ti)$ (figure 4(*c*)), and the n_{RFe} exchange constants deduced from T_C that are shown in figure

Table 3. The crystalline electric field coefficients A_{n0}, the values of $B_{20}\langle\hat{o}_{20}(J_z = J)\rangle$ at $T = 0$ K and the R–Fe exchange coefficient for R($Fe_{11}Ti$) (R = Tb, Dy, Ho and Er). The ratios of A_{44}/A_{40} and A_{64}/A_{60} are taken to be −2.4 and 1.6, respectively.

R in R($Fe_{11}Ti$)	A_{20} (K a_0^{-2})	A_{40} (K a_0^{-4})	A_{60} (K a_0^{-6})	n_{RFe} (μ_0)	$B_{20}\langle\hat{o}_{20}\rangle$ (K)	$B_{40}\langle\hat{o}_{40}\rangle$ (K)	$B_{60}\langle\hat{o}_{60}\rangle$ (K)
Tb	−61	−5.9	3.1	160	33.6	−7.1	−4.0
Dy	−61	−5.9	≥0.3	158	31.7	8.6	1.7
Ho	−61	−3.2	≤0.1	156	12.2	3.2	−1.0
Er	−61	−5.9	3.1	154	−11.6	−5.4	27.9

2(*b*), it is possible to deduce the temperature dependence of the rare-earth moment, and hence the anisotropy constants from (3). In the case of Gd, $J = S = \frac{7}{2}$ and there is no 4f contribution to the anisotropy. The magnetisation direction is determined by the iron anisotropy, K_1(Fe) which favours the *c* axis at all temperature, as for Y and Lu. For Tb, Dy and Ho, however, α_J is negative and the second-order term $B_{20}\langle\hat{o}_{20}\rangle$ favours the plane. The spin reorientation begins at the temperature where K_1(tot) (= K_1(Fe) + K_1(R)) changes sign. However, the reorientation may be extended over a wide temperature range according to the sign of K_2. The angle between the moment direction and the *c* axis, assuming both iron and rare-earth sublattices are coupled rigidly, is given by

$$\sin^2\theta = [-K_2 \pm (K_2^2 - 3K_1K_3)^{1/2}]/3K_3 \tag{8a}$$

or

$$\sin^2\theta = -K_1/2K_2 \tag{8b}$$

when K_3 can be neglected. Since K_3 depends only on the quantity $\langle\hat{o}_{60}\rangle$, which involves terms like J_z^6, it will be significant only for rare earths with a large spin moment, and below about 50 K.

The reorientation for Dy is the most straightforward [16]. It is evident from Mössbauer spectra on an oriented sample as a function of temperature. From the room-temperature spectra, we obtained a value of fitting angle $\Psi_{av} = 28°$ [19], which indicates the absorber is not fully oriented. The reorientation begins at about 210 K and it is complete at 80 K (figure 6), which behaviour can be reproduced with $A_{20} = -61$ K a_0^2 and $A_{40} = -5.9$ K a_0^{-4}. When A_{60} is greater than 0.3 K a_0^{-6} (table 3), the limiting value of θ is 90°; otherwise it is 69°. The agreement between the experimentally derived values of θ and the calculation is adequate, but it is unclear whether or not the magnetisation is exactly perpendicular to the *c* axis in the ground state. The temperature variations of θ and $K_1(R)$, $\bar{K}_2(R) = K_2(R) + K_2'(R)$ and $\bar{K}_3(R) = K_3(R) + K_3'(R)$ are shown in figures 10 and 11.

For Ho, it is deduced from the Mössbauer spectra of the oriented absorber that no change in magnetisation direction from the *c* axis occurs down to 15 K [19], which in comparison to Dy is explained by the small value of α_J for Ho. At $T = 0$, $B_{20}\langle\hat{o}_{20}\rangle$ is 12.2 K for Ho, compared with 31.7 K for Dy (table 3). A reduction of A_{40} and A_{60} is necessary to reproduce the absence of canting at low temperature (table 3). The calculated values of K_i are shown in figure 11.

The case of Tb is a little more complicated. The fourth-order Stevens coefficient β_J is positive (whereas for Dy and Ho it is negative), and K_2 is therefore negative. The spin

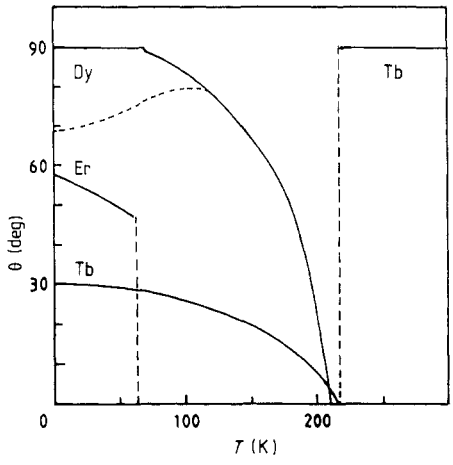

Figure 10. Calculation temperature variation of θ for R = Tb, Dy and Er. For $Dy(Fe_{11}Ti)$, the broken line corresponds to $A_{60} = 0$.

reorientation from the c axis to the plane is abrupt, and it takes place at about 450 K [19]. A second transition at lower temperature (220 K) is mainly due to the fourth-order term. The calculated values of K_i and θ are shown in figures 10 and 11. The spin reorientation is also manifest in the hyperfine field, which shows an anomaly at the iron sites (figure 9).

Turning now to the heavy rare earths with α_J positive, Er and Tm, it is predicted that the magnetisation direction lies along the c axis at all temperatures. But it was found, by Mössbauer spectroscopy [19] and magnetic measurements (figure 6), that the spin

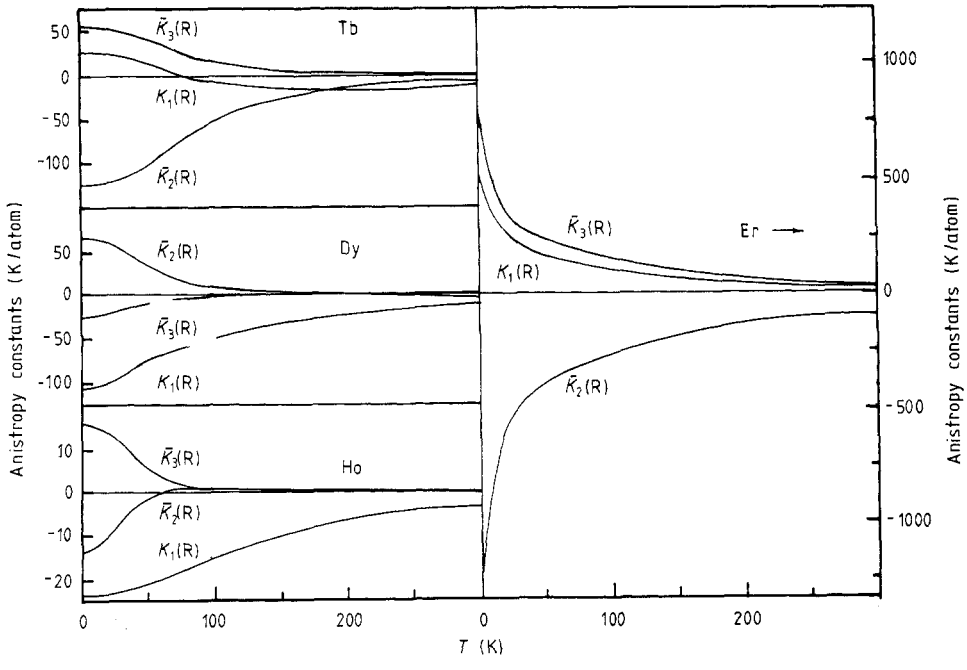

Figure 11. Calculated temperature variation of $K_i(R)$ for R = Tb, Dy, Ho and Er.

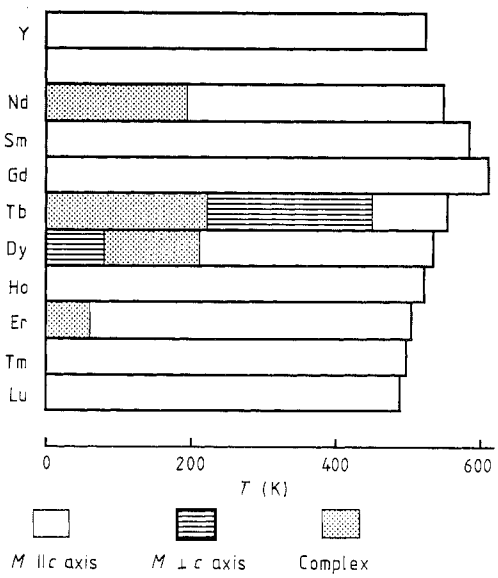

Figure 12. Temperature variation of the magnetic structure of the $R(Fe_{11}Ti)$ series.

reorientation appears below 60 K for Er, which may be understood by the relatively large positive value of $B_{60}\langle\hat{o}_{60}\rangle$ (table 3). The calculated values of K_i and θ are shown in figures 10 and 11. We have not found a spin reorientation for Tm above 80 K with Mössbauer spectroscopy.

The magnetic structures as a function of temperature in the $R(Fe_{11}Ti)$ family are summarised in figure 12.

4.5. Light rare earths

The Nd compound, according to the crystal-field parameters deduced from the dysprosium compound (table 3), should show the onset of a spin reorientation at about 190 K, since the value of $B_{20}\langle\hat{o}_{20}\rangle = 15.9$ K (at $T = 0$ K) is intermediate between Dy and Ho (table 3). This does seem to be observed at 200 K, in the magnetisation versus temperature curve measured in low field and shown in figure 6. However, we were unable to orient the samples properly at room temperature for x-ray diffraction or Mössbauer measurements. This may be due to the presence of a second phase, as mentioned in § 2.

Table 4. Intrinsic magnetic properties at room temperature.

	T_c (K)	K_1 (MJ m^{-3})	B_a (T)	$\mu_0 M_s$ (T)	$\mu_0 M_s^2/4$ kJ m^{-3}
$Y_2Fe_{14}B$	568	1.10	2.0	1.36	368
$Y(Fe_{11}Ti)$	524	0.89	2.0	1.12	250
$Nd_2Fe_{14}B$	592	5.05	9.1	1.60	509
$Sm(Fe_{11}Ti)$	584	4.87	10.5	1.14	259

The behaviour of the Sm compound is exceptional. If the $J = \frac{5}{2}$ multiplet alone were populated, the anisotropy field at room temperature would be 6.0 T compared with 10.5 T actually observed. In addition, the Stevens coefficient $\gamma_J = 0$ leads a zero value of K_3 (equation (3*d*)) so no sharp upturn should be observed in the magnetisation curve measured perpendicular to each direction. To explain these effects, it is necessary to take account of *J*-mixing [35], which adds in some of the $J = \frac{7}{2}$ excited state, leading to non-zero K_3 and a non-collinear spin structure.

5. Conclusions

(a) The series of iron-rich rare-earth intermetallic compounds $R(Fe_{11}Ti)$ exists with the $ThMn_{12}$ structure for the trivalent rare earths from Nd to Lu.

(b) The Curie point follows a trend similar to that in other rare-earth iron intermetallic series with a maximum at 607 K for R = Gd. Magnetic structures are ferrimagnetic for the heavy rare earths and ferromagnetic for the light rare earths.

(c) The iron moment is relatively small in the $ThMn_{12}$ structure. The average iron moment at $T = 0$ K is $1.7\mu_B$, and the largest moment is about $2.0\mu_B$ on 8*i* sites. The small iron moment may be a consequence of the short Fe–Fe distances of the nearest neighbours for 8*f* sites.

(d) The iron anisotropy at $T \simeq 0$ K, $K_1(Fe) \simeq 2.0$ MJ m^{-3}, is uniaxial and quite strong in comparison with that of $Y_2Fe_{14}B$. Spin reorientation transitions are found as a function of temperature for those rare earths with $\alpha_J < 0$. A set of crystal-field parameters has been derived to account for these transitions. A_{20} is opposite in sign and four or five times smaller than it is for the $R_2Fe_{14}B$ series.

(e) *J*-mixing must be taken into account in order to explain the substantial uniaxial anisotropy of $Sm(Fe_{11}Ti)$, and the first-order magnetisation process occurring in an applied field of 10 T below 130 K.

(f) A comparison of the intrinsic magnetic properties at room temperature of members of the $R(Fe_{11}Ti)$ and $R_2Fe_{14}B$ series is given in table 4. The quantity $\mu_0 M_s^2/4$ represents the theoretical upper limit on the energy product that could be achieved for a magnet made from the alloy. Apart from the lower magnetisation of the $ThMn_{12}$-structure compounds, the other intrinsic magnetic properties are quite similar.

(g) Unlike $Nd_2Fe_{14}B$, there is little prospect of increasing B_a (the theoretical upper limit for the coercivity) by rare-earth substitution in $Sm(Fe_{11}Ti)$. T_C can be increased in either compound by cobalt substitution [6].

(h) $Sm(Fe_{11}Ti)$ is likely to become a serious candidate as an alloy for making moderately high-performance permanent magnets if useful coercivity can be developed, particularly in precipitation-hardened alloys or in oriented melt-spun ribbons.

Acknowledgments

This work forms part of the 'Concerted European Action on Magnets', a project supported by the Commission of the European Communities. We are grateful to Dr Jos Perenboom for making it possible for us to use the facilities at the High Field Magnet Laboratory of the University of Nijmegen, to Dominique Givord and Lu Quan of the Laboratoire Louis Néel, and the Service National des Champs Intenses, Grenoble.

References

[1] Sagawa M, Fujimura S, Togawa M, Yamamoto H and Matsuura Y 1984 *J. Appl. Phys.* **55** 2083
[2] Herbst J F, Croat J J, Pinkerton F E and Yelon W B 1984 *Phys. Rev.* B **29** 4176
[3] Mitchell I V (ed.) 1985 *Nd–Fe Permanent Magnets—Their Present and Future Applications* (London: Elsevier)
[4] De Mooij D B and Buschow K H J 1987 *Philips J. Res.* **42** 246
[5] De Boer F R, Hung Ying-Kai, De Mooij D B and Buschow K H J 1987 *J. Less-Common Met.* **135** 199
[6] Buschow K H J, de Mooij D B, Brouha M, Smit H H A and Thiel R C 1988 *IEEE Trans. Magn.* **MAG-24** 1161
[7] Wang Xian-Zhong, Chevalier B, Berlureau T, Etouerneau J, Coey J M D and Cadogan J M 1988 *J. Less-Common Met.* **138** 235
[8] Yang Ying-Chang, Wang Lin-Shu, Sun Shu-He and Gu Dong-Mei 1988 *J. Appl. Phys.* **63** 3702
[9] Hadjipanayis G C, Aly S H and Cheng Shu-Fan 1987 *Appl. Phys. Lett.* **51** 2048
[10] Givord D, Li H S and Perier de la Bâthie R 1984 *Solid State Commun.* **51** 857
[11] Moze O, Pareti L, Solzi M and David W I F 1988 *Solid State Commun.* **66** 465
[12] Hutchings M T 1964 *Solid State Phys.* **16** 227 (New York: Academic)
[13] Rudowicz C 1985 *J. Phys. C: Solid State Phys.* **18** 1415
[14] Cadogan J M, Gavigan J P, Givord D and Li H S 1988 *J. Phys. F: Met. Phys.* **18** 779
[15] Sinnema S, Radwanski R J, Franse J J M, de Mooij D B and Buschow K H J 1984 *J. Magn. Magn. Mater.* **44** 333
[16] Li Hong-Shuo, Hu Bo-Ping and Coey J M D 1988 *Solid State Commun.* **66** 133
[17] Hiroyoshi H, Kato H, Yamada M, Saito N, Nagawa Y, Hirosawa S and Sagawa M 1987 *Solid State Commun.* **62** 475
[18] Gavigan J P, Li Hong-Shuo, Coey J M D, Cadogan J M and Givord D 1989 *J. Physique* at press
[19] Hu Bo-Ping, Li Hong-Shuo and Coey J M D 1989 *Hyperfine Interact.* at press
[20] Buschow K H J 1977 *Rep. Prog. Phys.* **40** 1179
[21] Burzo E, Oswold E, Huang M Q, Boltich E and Wallace W E 1985 *J. Appl. Phys.* **57** 4109
[22] Belorizky E, Fremy M A, Gavigan J P, Givord D and Li H S 1987 *J. Appl. Phys.* **61** 3971
[23] Li Hong-Shuo and Hu Bo-Ping 1988 *Proc. Int. Conf. Magnetism (Paris) 1988*
[24] Gubbens P C M, van Appeldorn J H F, van der Kraan A M and Buschow K H J 1974 *J. Phys. F: Met. Phys.* **4** 921
[25] Shimizu M and Inoue S 1987 *J. Magn. Magn. Mater.* **70** 61
[26] Helmheldt R B, Vleggaar J J M and Buschow K H J 1988 *J. Less-Common Met.* **138** L11
[27] Coey J M D and Ryan D H 1984 *IEEE Trans. Magn.* **MAG-2** 1278
[28] Bolzoni F, Gavigan J P, Givord D, Li H S, Moze O and Pareti L 1987 *J. Magn. Magn. Mater.* **66** 158
[29] Bushow K H J and Grössinger R 1987 *J. Less-Common Met.* **135** 39
[30] Bogé M, Czjzek L G, Givord D, Jeandey C, Li H S and Oddou J L 1986 *J. Phys. F: Met. Phys.* **16** L67
[31] Schmitt D 1979 *J. Phys. F: Met. Phys.* **9** 1975, 1979
[32] March N H 1957 *Adv. Phys.* **6** 1
[33] Torrens I M 1972 *Interatomic Potentials* (New York: Academic) p 35
[34] Newman D J 1971 *Adv. Phys.* **20** 197
[35] De Wijn H W, van Diepen A M and Buschow K H J 1976 *Phys. Status Solidi* b **76** 11